Determination of ^{13}C Chemical Shift Tensors in the Presence of Hydrogen Bonding and ^{14}N Quadrupolar Coupling: *p*-Aminosalicylic Acid, Isoniazid, and Pyrazinamide

Dewey H. Barich, Jacalyn S. Clawson, Dirk Stueber, Mark Strohmeier, Ronald J. Pugmire, and David M. Grant*

Department of Chemistry, University of Utah, Salt Lake City, Utah 84112

Received: July 12, 2002

The ^{13}C chemical-shift tensor principal values were measured for *p*-aminosalicylic acid, pyrazinamide, and isoniazid. A moderate-strength hydrogen bond between adjacent *p*-aminosalicylic acid molecules in the crystal was simulated several different ways in attempts to find a reasonable model of the electrostatic interactions in the crystal. Crystal lattice effects on the calculated chemical-shift tensors are treated by application of the embedded ion method (EIM). Coupling between ^{14}N and several ^{13}C atoms was included in the data analysis to provide more accurate ^{13}C chemical-shift tensor principal values. The chemical-shift tensors are assigned with a permutative algorithm based upon the computed chemical shifts.

Introduction

Knowledge of a material's structure is of great importance in the development of pharmaceutical materials. X-ray crystallography is often the preferred means of structural determination. When crystals of suitable size for X-ray analysis are unavailable, alternative structural data sources may be needed. Solid-state NMR of crystalline samples is complementary to X-ray structural determinations, as it provides information about the local structure of the molecules, as well as information about the crystallographic unit cell, e.g., the number of molecules per crystallographic asymmetric unit.

Obtaining chemical-shift tensor (CST) principal values from natural abundance samples with a relatively large number of carbon atoms can prove difficult because individual sideband patterns crowd the spectrum considerably. Moreover, the possibility of sidebands from different sideband patterns overlapping one another becomes quite high, which complicates data analysis. This task is made tractable in this study by employing the FIREMAT experiment[1,2] to associate individual spinning sideband patterns with their respective isotropic chemical shift. A spinning sideband pattern is extracted for each resolvable isotropic chemical shift. In favorable cases individual sets of principal values are obtained for accidentally overlapped isotropic shifts.

Comparing predicted CST data to experimental values provides a means of determining molecular conformation in a crystal. Harper, et al.,[3] have recently predicted the relative stereochemistry of the natural product terrein by comparing computed CST data of different structural models to solid-state NMR data. Similar efforts enabled the prediction of the magnitude of the inter-ring angle and librational motion of individual molecules in crystalline biphenyl.[4]

The present study reports the ^{13}C CST principal values of three pharmaceuticals that are used to treat tuberculosis. Each molecule is shown with the heavy numbering scheme utilized in this work. Each of these molecules contains ^{14}N, whose presence complicates ^{13}C solid-state NMR spectra due to the dipolar coupling between the observed ^{13}C and the adjacent ^{14}N nucleus. Hence, the analysis of ^{14}N-coupled carbon peaks in these FIREMAT spectra utilized a recent addition to our in-house data analysis software that incorporates these quadrupolar−dipolar interactions.[5] The mathematical description of the $^{13}C-^{14}N$ coupling is incompatible with the criteria for applying TIGER processing,[6] hence all experimental data reported in this study were fit directly from the 2D FIDs.

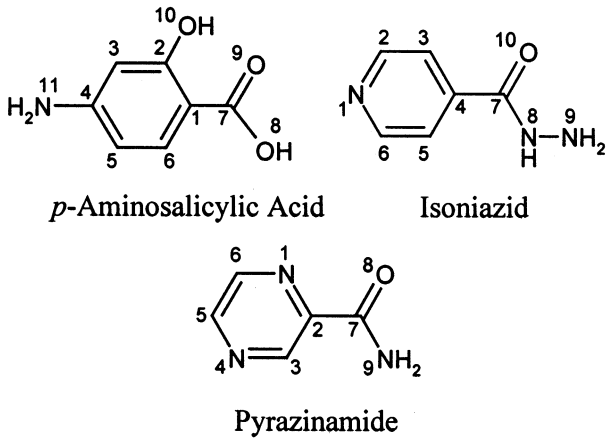

p-Aminosalicylic Acid Isoniazid

Pyrazinamide

To calculate accurate chemical shifts in crystals, it is important to include crystal lattice effects, particularly when intermolecular electrostatic interactions are significant, as was recently found with the DNA bases by Stueber and Grant.[7] This too is the case for the crystalline form of *p*-aminosalicylic acid in which there is an intramolecular hydrogen bond between O10 and O9. Also, O8 and O9 of two neighboring molecules form a pair of intermolecular hydrogen bonds in which the carboxylic acid group serves as both donor and acceptor. This dimer moiety thus contains a total of four hydrogen bonds. An inversion center located at the center of the dimer makes the two intramolecular hydrogen bonds and the two intermolecular hydrogen bonds equivalent. Each of these hydrogen bonds is classified by Jeffrey[8] as a moderate hydrogen bond (Table 1), a mostly electrostatic interaction. Since O9 is involved in both the intermolecular and intramolecular hydrogen bonds, it is reason-

* Corresponding author.

10.1021/jp021604n CCC: $22.00
Published on Web 10/30/2002

TABLE 1: Hydrogen Bond Classification Parameters[8]

	strong	moderate	weak
A−H···B interaction	mostly covalent	mostly electrostatic	electrostatic
A···B bond lengths (Å)	2.2−2.5	2.5−3.2	3.2−4.0
bond angles (°)	175−180	130−180	90−150

able to expect that some treatment of the intermolecular interaction would be needed to accurately predict the CST data, particularly for C2 and C7.

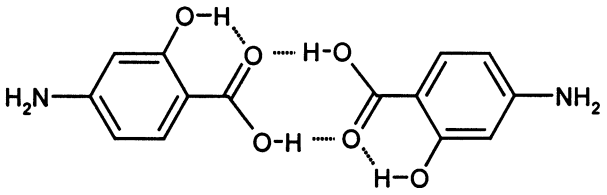

Lattice treatments are sometimes attempted with cluster models to simulate the electrostatic crystal lattice effects of adjacent molecules surrounding a molecule of interest.[9−11] While this approach treats intermolecular effects, and thus in principle improves agreement between theory and experiment, it has some drawbacks. First, the finite nature of cluster models limits their effectiveness in modeling an infinite lattice where electrostatic forces converge rather slowly as the distance increases. Second, the addition of molecules to the model adds exponentially to the computational expense. An alternative to cluster models is the use of point charge arrays to model the environment. Oldfield and de Dios developed the charge field perturbation (CFP) approach, which uses a force field to calculate a point charge array that surrounds an embedded molecule or molecular fragment that is to be treated quantum mechanically.[12,13] This approach exhibited considerable improvement between computed and measured NMR data. The calculation of electrostatic potentials over an infinite periodic lattice is difficult to achieve over a finite volume. Ewald[14] solved this well-known problem by simulating the Madelung potential via a lattice summation. Truong has used the Ewald summation method to study electrostatic effects in both macromolecules and crystals,[15−17] and a recent approach reported by Klintenberg, Derenzo, and Weber,[18] (KDW) generates a finite point charge array that simulates the Madelung potential at its center by fitting the charges that are outside an inner region to reproduce the Madelung potential. Hence, this method accommodates the effects of an infinite lattice, making it applicable to crystalline systems. The KDW program[18] was modified in this laboratory by Stueber et al.[19] to accommodate partial atomic charges in neutral as well as ionic species, and was incorporated into a computational scheme named the embedded ion method (EIM). This model improves some of the aforementioned cluster model features. It only requires a known crystal structure because the partial charges at crystallographic atomic positions are calculated with quantum chemistry programs and made self-consistent by cycling between successive approximations to the electrostatic lattice fields. The crystal structures of all three molecules studied here are known. Pyrazinamide[20] crystallizes in the $P2_1/n$ space group, *p*-aminosalicylic acid[21] crystallizes in the $P2_1/c$ space group, and isoniazid crystallizes[22] in the $P2_12_12_1$ space group. Each material has four molecules in the unit cell.

The improvement exhibited by the EIM between theory and experiment for a series of ionic carbonates and thiocarbonates[19,23] has been documented. How well the EIM models weaker intermolecular interactions is incompletely understood and is one focal point of this study. On the basis of the geometrical criteria described above, this moderate hydrogen bond in *p*-aminosalicylic acid is the strongest such interaction in the crystalline materials studied here. As such, it was studied separately in greater detail than the other two molecules to determine what modeling efforts are needed to characterize the hydrogen bonding present in the materials in this work.

Methods

Materials. Isoniazid (4-pyridinecarboxylic acid hydrazide), pyrazinamide (pyrazine-2-carboxylic acid amide), and *p*-aminosalicylic acid as the free acid (4-amino-2-hydroxybenzoic acid) were obtained from Sigma and used without purification. X-ray powder diffraction verified that the polymorphic form of each material matched that of the X-ray structure used in the calculations.

NMR Spectroscopy. All ^{13}C spectra were collected on a CMX-400 NMR spectrometer operating at 400.12 MHz for ^1H and 100.62 MHz for ^{13}C. All spectra are referenced to TMS via a secondary external reference to the high-frequency peak of adamantane at 38.56 ppm. Signal enhancement via cross-polarization was accomplished with optimal contact times of 3.0 ms (isoniazid and pyrazinamide) and 5.0 ms (*p*-aminosalicylic acid). The ^1H T_1 of each sample was determined via saturation recovery to be 180, 320, and 80 s for isoniazid, pyrazinamide, *p*-aminosalicylic acid, respectively. The optimal recycle delay for each material was determined so that signal-to-noise was maximized for a constant experimental time.

The following FIREMAT parameters were used for all three molecules in this study. The acquisition and evolution spectral widths were 92160 and 15360 Hz, respectively. The sample spinning speed was 1920 Hz. Eight evolution increments were collected. There were 48 acquisition points per rotor period. A flip-back pulse was employed for all FIREMAT spectra. Other parameters were as follows. *p-Aminosalicylic acid*: The $\pi/2$ pulse width for ^1H was 4.10 μs while the π pulse for ^{13}C was 8.4 μs. Each increment was the sum of 384 transients. The optimal constant-time recycle delay was 45 s. *Isoniazid*: The $\pi/2$ pulse width for ^1H was 4.15 μs. The π pulse for ^{13}C was 8.5 μs. The FID of each increment was the sum of 672 transients. The optimal recycle delay to maximize signal-to-noise in a given experimental time was 60 s. *Pyrazinamide*: The $\pi/2$ pulse width for ^1H was 4.25 μs. The π pulse for ^{13}C was 8.6 μs. A total of 384 transients was collected in each increment. The optimal constant-time recycle delay was 60 s. A dipolar dephased FIREMAT was also collected with a dipolar dephasing time of 22 μs and with 864 scans collected per increment, sharing all other parameters with the cross polarization FIREMAT.

Spectral Analysis. Data were transferred to a Sun computer for analysis. A version of our in-house software that incorporates the effects of coupling a spin-1/2 to a spin-1 nucleus was used to fit each spectrum.[5] For the carbons that are coupled to ^{14}N, it was assumed that the δ_{33} principal component of the chemical shift tensor was perpendicular to the molecular plane. The simulated spectrum was generated by adding the model used for each peak in the spectrum.

Calculations. All quantum calculations were performed with *Gaussian 98*[24] at the B3LYP/D95** level of theory.[25,26] The chemical shift calculations employed the gauge-including atomic orbitals (GIAO) ansatz.[27,28]

Isolated Molecules. Prior to calculating the CST data, the proton positions from the X-ray crystal structures were refined. This was done for isoniazid, pyrazinamide, and *p*-aminosalicylic acid as well as for a hydrogen-bonded dimer of *p*-aminosalicylic

TABLE 2: EIM Parameters

molecule	N_A	N_B	N_C	zone 2	zone 1
p-aminosalicylic acid monomer	4	5	2	400	90
p-aminosalicylic acid dimer	4	5	2	500	300
isoniazid	4	4	4	500	60
pyrazinamide	4	4	4	500	60

acid in which the carboxylic acid of each molecule serves as both proton donor and acceptor (vide supra).

Embedded Ion Method. The EIM has been described previously.[19] Details of the calculations are supplied in Table 2. The model was applied to *p*-aminosalicylic acid, isoniazid, pyrazinamide, and the *p*-aminosalicylic acid dimer. The point charge array is constructed by replicating a number of unit cells in the *a*, *b*, and *c* directions (labeled N_A, N_B, and N_C, respectively). The point charge array consists of three zones. The innermost zone (zone 1) contains all atomic positions that are part of the embedded molecule as well as some other atomic positions. Zone 2 envelops zone 1, and the zone 2 entries in Table 2 include the zone 1 atom count. All other point charges constitute zone 3, and only these charges are altered to simulate the Madelung potential. For the EIM work the proton refinement was performed inside the point charge array created by the KDW program at each iterative step. A new point charge array was generated following each proton optimization until each atomic charge value in the embedded molecule was less than 0.001 *e* from that of the previous point charge array, i.e., until the NBO[29,30] atomic charges became self-consistent. Once atomic charge self-consistency was achieved, the chemical shift data were calculated.

Spectral Assignments. Some assignments were possible solely on the basis of experimental data. For example, the quaternary carbons of pyrazinamide (C2 and C7) were unambiguously identified on the basis of the dipolar dephasing experiment, and each peak identified by its isotropic chemical shift. With the quaternary carbon peaks identified, only the CH carbons (C3, C5, and C6) required the aid of the computed shieldings. A modified version (that uses only principal values not full tensors) of a previously reported assignment procedure[31] was applied. The assignment process, when applied to the *p*-aminosalicylic acid, resulted in a highly confident scheme even without separating out the quaternary peaks. The second-best assignment scheme in this case could be ruled out with more than 98% confidence.

Converting Shieldings to Shifts. The computed shieldings for the EIM-based isoniazid, pyrazinamide, and the *p*-aminosalicylic acid monomer were plotted against the experimental shifts. This procedure was repeated for the three isolated molecules. The shielding values were converted to the shift scale via the corresponding least-squares regression equation. The root-mean-square difference between the converted shieldings and the best-fit line was computed. The same procedure was applied to all four *p*-aminosalicylic acid models (vide infra).

Results

The FIREMAT isotropic guide spectrum of each molecule is presented in Figure 1; all reported principal values were obtained from direct analysis of the 2D FIDs. Figures 2, 3, and 4 portray the first increments in the evolution dimension of the ^{13}C FIREMAT spectra of *p*-aminosalicylic acid, pyrazinamide, and isoniazid, respectively. Subsequent increments are not shown because the phase-encoding nature of the FIREMAT experiment prevents simultaneous phasing of all the sub-spectra.

Table 3 reports the measured CST data for all three molecules. Table 4 contains the differences between the predicted and experimental values of the four *p*-aminosalicylic acid models. Table 5 reports the calculated EIM CST values for all three molecules.

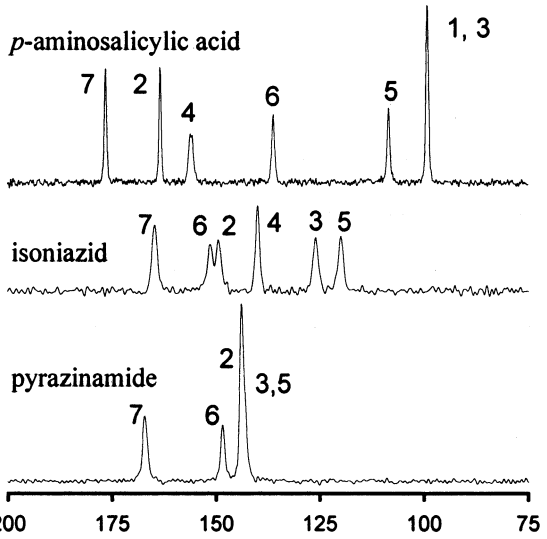

Figure 1. ^{13}C FIREMAT guide spectra of *p*-aminosalicylic acid (top), isoniazid (middle), and pyrazinamide (bottom). All spectra are plotted without line broadening.

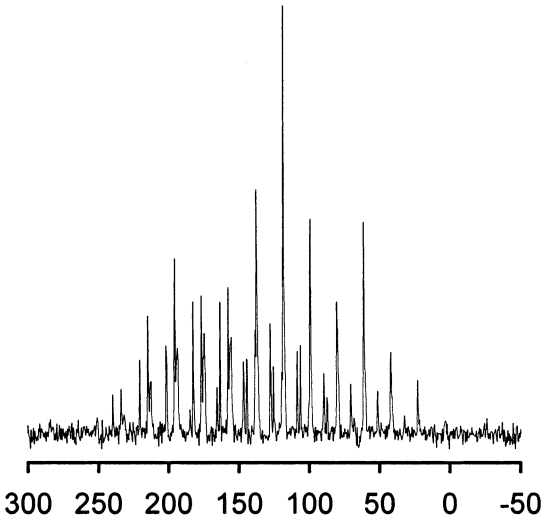

Figure 2. First increment of the ^{13}C FIREMAT spectrum of *p*-aminosalicylic acid.

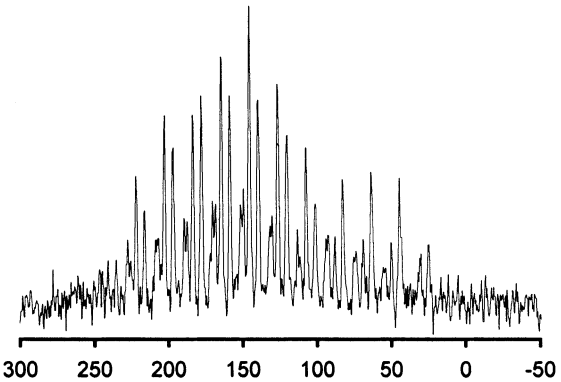

Figure 3. First increment of the ^{13}C FIREMAT spectrum of isoniazid.

Discussion

Lattice Effects. As mentioned earlier, before a comparison of experiment and theory for all three molecules in this study

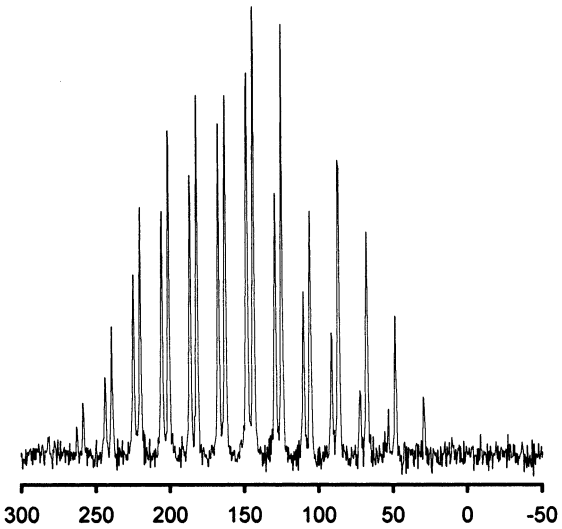

Figure 4. First increment of the ^{13}C FIREMAT spectrum of pyrazinamide.

TABLE 3: ^{13}C FIREMAT Chemical-Shift Tensor Principal Values[a]

molecule	carbon	δ_{11}	δ_{22}	δ_{33}	δ_{iso}	δ_{span}[b]	δ_{acen}[c]
p-aminosalicylic acid	1	153.6	126.4	17.1	99.0	136.5	41.1
	2	249.0	174.0	66.9	163.3	182.1	16.0
	3	152.4	111.2	32.4	98.7	120.0	18.8
	4	240.5	188.4	38.8	155.9	201.6	48.7
	5	185.1	119.4	20.4	108.3	164.7	16.6
	6	233.0	163.2	11.9	136.0	221.1	40.7
	7	240.5	184.2	104.7	176.5	135.9	11.6
isoniazid	2	250.9	161.0	35.8	149.2	215.1	17.6
	3	223.9	146.5	7.3	125.9	216.6	30.9
	4	239.3	160.6	19.6	139.8	219.7	31.2
	5	214.9	135.4	9.0	119.8	205.9	23.5
	6	255.9	157.9	40.1	151.3	215.8	9.9
	7	247.1	154.1	92.7	164.7	154.4	−15.8
pyrazinamide	2	246.2	138.4	47.0	143.9	199.3	−8.2
	3,5[d]	243.9	158.0	28.5	143.4	215.4	21.8
	6	251.4	156.5	37.0	148.3	214.4	12.3
	7	243.2	163.5	94.5	167.1	148.7	−5.4

[a] All values are given in ppm. [b] Span = $\delta_{11} - \delta_{33}$. [c] Acentricity = $\delta_{22} - (\delta_{11} + \delta_{33})/2$. [d] C3 and C5 were indistinguishable in the experiment.

can be completed, the issue of how to treat the intermolecular hydrogen bond in *p*-aminosalicylic acid must be resolved. Of the four *p*-aminosalicylic acid models used in the calculations, only the isolated monomer neglects any treatment of the intermolecular hydrogen bond. Not surprisingly, the isolated monomer calculations exhibit poor agreement with the experimental results for both C2 (δ_{22}) and C7 (δ_{11} and δ_{22}). The isolated dimer reduces the RMS by 31% and is especially effective in improving the agreement at C7. It achieves only small improvements for C2, presumably since the major hydrogen bonding effects on C2 arise from the intramolecular hydrogen bond interaction that is present and treated in both models. This suggests that the shortcomings of the theory for C2 are due to other long-range intermolecular interactions with the surrounding lattice, and establishes the need to treat the entire lattice. Either model (monomer or dimer) treated with the EIM shows remarkable improvements; the RMS of each improves nearly 20% compared to the isolated dimer model. The RMS values for these two EIM-based models are indistinguishable, thus the simpler EIM monomer model represents *p*-aminosalicylic acid in the combined plot of EIM calculated vs experimental principal values discussed below. The fact that the EIM-based monomeric and dimeric models are statistically indistinguishable is not surprising. It suggests that there is not a significant amount of covalent interaction between the hydrogen and the acceptor oxygen. This is consistent with the categorization of Jeffrey that moderate hydrogen bonds are mostly electrostatic in nature.

TABLE 4: Differences[a] Between Computed and Measured Values[b] of the Four *p*-Aminosalicylic Acid Models

	carbon	isolated monomer	isolated dimer	EIM dimer	EIM monomer
δ_{11}	1	0.2	−1.6	−9.5	−8.8
	2	−1.5	−1.3	0.6	0.0
	3	8.6	7.2	3.9	4.6
	4	−0.7	−1.3	−3.1	−3.0
	5	−5.1	−5.0	−0.2	0.9
	6	4.1	5.6	8.1	6.6
	7	21.4	4.0	1.8	3.9
δ_{22}	1	0.6	2.1	0.4	−1.8
	2	19.1	16.4	3.6	4.7
	3	−7.8	−9.2	−15.4	−14.6
	4	−8.0	−8.1	2.8	5.5
	5	−14.4	−14.8	−7.2	−5.6
	6	−9.2	−7.0	−3.3	−4.5
	7	−21.0	4.1	5.0	0.9
δ_{33}	1	1.5	2.0	2.8	2.6
	2	1.6	1.2	2.4	2.5
	3	1.3	0.2	2.1	2.2
	4	−2.2	−3.1	−1.2	−2.1
	5	5.9	5.0	4.3	4.6
	6	7.2	4.9	4.1	4.9
	7	−1.5	−1.4	−1.8	−3.3
RMS		9.5	6.6	5.3	5.2

[a] Differences are computed minus measured values. [b] All values are given in ppm.

TABLE 5: Computed Chemical-Shift Tensor Principal Values from EIM[a]

molecule	carbon	δ_{11}	δ_{22}	δ_{33}	δ_{iso}	δ_{span}[b]	δ_{acen}[c]
p-aminosalicylic acid	1	140.9	121.2	18.7	93.6	122.3	41.4
	2	242.9	174.2	67.2	161.4	175.7	19.2
	3	153.0	93.8	33.3	93.4	119.6	0.7
	4	231.3	190.2	34.4	152.0	196.9	57.3
	5	181.3	110.6	23.9	105.3	157.4	8.1
	6	233.7	154.6	15.8	134.7	217.9	29.8
	7	238.4	180.4	98.5	172.4	139.9	11.9
isoniazid	2	255.8	161.2	39.3	152.1	216.5	13.7
	3	231.1	140.5	6.4	126.0	224.6	21.7
	4	235.6	162.1	18.2	138.6	217.3	35.2
	5	219.0	126.1	11.5	118.9	207.5	10.9
	6	259.4	160.5	37.9	152.6	221.6	11.8
	7	247.6	160.2	93.0	167.0	154.6	−10.1
pyrazinamide	2	248.5	152.5	41.9	147.6	206.6	7.3
	3	253.9	158.9	37.2	150.0	216.7	13.3
	5	252.6	161.0	36.0	149.8	216.6	16.7
	6	250.8	164.7	37.8	151.1	213.1	20.4
	7	248.2	166.9	88.0	167.7	160.2	−1.2

[a] All values are given in ppm. [b] Span = $\delta_{11} - \delta_{33}$. [c] Acentricity = $\delta_{22} - (\delta_{11} + \delta_{33})/2$.

Comparing Experiment and Theory. Both isoniazid and pyrazinamide exhibit hydrogen bonding in the crystal lattice that is modestly weaker than that found in *p*-aminosalicylic acid, based on Jeffrey's criteria[8] (Table 1). Based on this, these two molecules are treated solely as monomers in the EIM. Computations of each show significant improvement in agreement with experiment when the EIM model is employed. With the best model of the *p*-aminosalicylic acid (vide supra) identified, the EIM computed results of all three molecules were plotted together to obtain a best-fit line to convert the computed shieldings to the experimental chemical shift scale. Figure 5

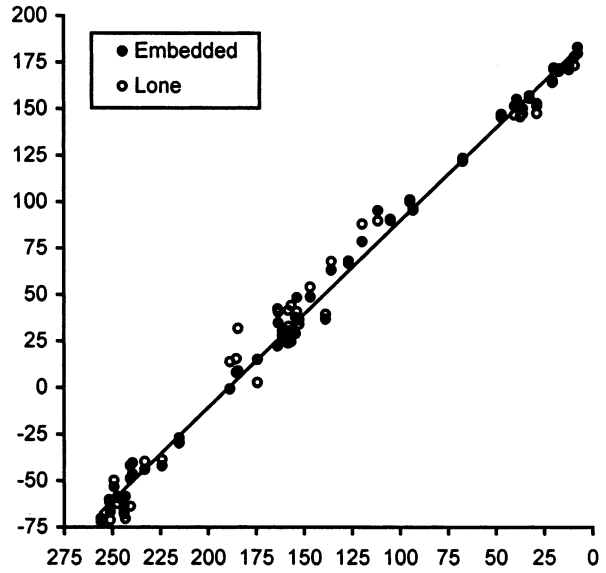

Figure 5. Plot of computed shieldings in ppm from bare nucleus (ordinate) vs measured chemical shifts in ppm from TMS (abscissa). The best-fit line of the EIM-based computed values is shown.

shows the plot for both the EIM and the isolated molecules, with the best-fit line for the EIM-based models included. The overall RMS difference between the EIM-computed values and the best-fit line is 5.9 ppm. For the computed data on the isolated molecules the RMS difference is 9.3 ppm. A statistical *F*-test yields a 0.1% probability that data calculated for the isolated molecules provides a fit of experimental data that is as good as the EIM-based results. In addition to the improved correlation of theory and experiment offered by the EIM, the EIM also provides an improved means of modeling hydrogen bonding interactions that arise largely from electrostatic interaction.

Effect of ^{14}N on Measured ^{13}C Tensor Principal Values. The residual dipolar $^{13}C-^{14}N$ coupling complicates spectral analysis. The coupling magnitude (in Hz) is field independent but the magnitude of chemical-shift anisotropy is field dependent (in Hz). While it is common to simply collect data at the highest available field and otherwise ignore the coupling, the CST principal values can differ in principle from the "apparent" values by several ppm.[5] The interaction has been accommodated here for carbons that are coupled to ^{14}N nuclei. In the molecules reported here, the effects of the coupling are relatively modest as may be seen in the spectra in Figure 1. Of the nine carbons in this study that exhibit this coupling, only δ_{33} of C2 and C3 in pyrazinamide change by more than 2.0 ppm (i.e., 4.2 and 2.8 ppm, respectively).

Conclusions

Significant improvements in the accuracy of calculated ^{13}C chemical shifts of hydrogen-bonded systems were achieved by simulating the crystal lattice with the EIM. Given that the hydrogen bonds in *p*-aminosalicylic acid lie near the boundary of moderate and strong hydrogen bonds,[8] it seems likely that the EIM will work for those hydrogen bonds that arise largely from electrostatic interactions, i.e., weak and moderate hydrogens bonds in Jeffrey's classifications. Proper application of the EIM to systems with hydrogen bonds which exhibit greater intermolecular covalent character than the examples studied here may need to include neighboring molecules in the quantum mechanical core of the EIM, rather than the typical use of only a single molecule. Further work is necessary to better understand the general applicability of the EIM on hydrogen-bonded systems.

Acknowledgment. This work was supported by the National Institute of Health under Grant GM 08521-40. Computer resources were provided by the Center for High Performance Computing at the University of Utah. The authors gratefully acknowledge D. W. Alderman for many insightful and helpful discussions in the course of this work.

References and Notes

(1) Alderman, D. W.; McGeorge, G.; Hu, J. Z.; Pugmire, R. J.; Grant, D. M. *Mol. Phys.* **1998**, *95*, 1113−1126.

(2) McGeorge, G.; Hu, J. Z.; Mayne, C. L.; Alderman, D. W.; Pugmire, R. J.; Grant, D. M. *J. Magn. Reson.* **1997**, *129*, 134−144.

(3) Harper, J. K.; Mulgrew, A. E.; Barich, D. H.; Li, J. Y.; Strobel, G.; Grant, D. M. *J. Am. Chem. Soc.* **2001**, *123*, 9837−9842.

(4) Barich, D. H.; Pugmire R. J.; Grant D. M.; Iuliucci, R. J. *J. Phys. Chem. A* **2001**, *105*, 6780−6784.

(5) Strohmeier, M.; Alderman, D. W.; Grant, D. M. *J. Magn. Reson.* **2002**, *155*, 263−277.

(6) McGeorge, G.; Hu, J. Z.; Mayne, C. L.; Alderman, D. W.; Pugmire, R. J.; Grant, D. M. *J. Magn. Reson.* **1997**, *129*, 134−144.

(7) Stueber, D.; Grant, D. M. *J. Am. Chem. Soc.* **2002**, *124*, 10539−10551.

(8) Jeffrey, G. A. *An Introduction to Hydrogen Bonding*; Oxford University Press: New York, 1997.

(9) de Dios, A. C.; Oldfield, E. *Solid State NMR* **1996**, *6*, 102−125.

(10) Ferraro, M. B.; Repetto, V.; Facelli, J. C. *Solid State NMR* **1998**, *10*, 185−189.

(11) Orendt, A. M.; Facelli, J. C.; Grant, D. M. *Chem. Phys. Lett.* **1999**, *302*, 499−504.

(12) de Dios, A. C.; Oldfield, E. *Chem. Phys. Lett.* **1993**, *205*, 108−116.

(13) de Dios, A. C.; Pearson, J. G.; Oldfield, E. *Science* **1993**, *260*, 1491−1495.

(14) Ewald, P. *Ann. Phys.* **1921**, *64*, 253−287.

(15) Stefanovich, E. V.; Truong, T. N. *J. Phys. Chem. B* **1998**, *102*, 3018−3022.

(16) Vollmer, J. M.; Stefanovich, E. V.; Truong, T. N. *J. Phys. Chem. B* **1999**, *103*, 9415−9422.

(17) Vollmer, J. M.; Truong, T. N. *J. Phys. Chem. B* **2000**, *104*, 6308−6312.

(18) Klintenberg, M.; Derenzo, S. E.; Weber, M. J. *Comput. Phys. Commun.* **2000**, *131*, 120−128.

(19) Stueber, D.; Guenneau, F. N.; Grant, D. M. *J. Chem. Phys.* **2001**, *114*, 9236−9243.

(20) Tiwari, R. K.; Patel, T. C.; Singh, T. P. *Indian J. Phys.* **1982**, *56A*, 413−419.

(21) Lin, C.-T.; Siew, P.-Y.; Byrn, S. R. *J. Chem. Soc., Perkin II* **1978**, 957−962.

(22) Bhat, T. N.; Singh, T. P.; Vijayan, M. *Acta Crystallogr.* **1974**, *B30*, 2921−2922.

(23) Stueber, D.; Orendt, A. M.; Facelli, J. C.; Parry, R. W.; Grant, D. M. *Solid State NMR* **2002**, *22*, 29−49.

(24) Frisch, M. J.; Trucks, G. W.; Schlegel, H. B.; Scuseria, G. E.; Robb, M. A.; Cheeseman, J. R.; Zakrzewski, V. G.; Montgomery, J. A., Jr.; Stratmann, R. E.; Burant, J. C.; Dapprich, S.; Millam, J. M.; Daniels, A. D.; Kudin, K. N.; Strain, M. C.; Farkas, O.; Tomasi, J.; Barone, V.; Cossi, M.; Cammi, R.; Mennucci, B.; Pomelli, C.; Adamo, C.; Clifford, S.; Ochterski, J.; Petersson, G. A.; Ayala, P. Y.; Cui, Q.; Morokuma, K.; Salvador, P.; Dannenberg, J. J.; Malick, D. K.; Rabuck, A. D.; Raghavachari, K.; Foresman, J. B.; Cioslowski, J.; Ortiz, J. V.; Baboul, A. G.; Stefanov, B. B.; Liu, G.; Liashenko, A.; Piskorz, P.; Komaromi, I.; Gomperts, R.; Martin, R. L.; Fox, D. J.; Keith, T.; Al-Laham, M. A.; Peng, C. Y.; Nanayakkara, A.; Challacombe, M.; Gill, P. M. W.; Johnson, B.; Chen, W.; Wong, M. W.; Andres, J. L.; Gonzalez, C.; Head-Gordon, M.; Replogle, E. S.; Pople, J. A. *Gaussian 98* (Revision A.11); Gaussian, Inc.: Pittsburgh, PA, 2001.

(25) Becke, A. D. *J. Chem. Phys.* **1993**, *98*, 5648−5652.

(26) Lee, C.; Yang, W.; Parr, R. G. *Phys. Rev. B* **1988**, *37*, 785−789.

(27) Ditchfield, R. *Mol. Phys.* **1974**, *27*, 789−807.

(28) Wolinski, K.; Hinton, J. F.; Pulay, P. *J. Am. Chem. Soc.* **1990**, *112*, 8251−8260.

(29) NBO Version 3.1; Glendening, E. D.; Reed, A. E.; Carpenter, E.; Weinhold, F.

(30) Reed, A. E.; Weinstock, R. B.; Weinhold F. *J. Chem. Phys.* **1984**, *83*, 735.

(31) Liu, F.; Phung, C. G.; Alderman, D. W.; Grant, D. M. *J. Magn. Reson.* **1996**, *120*, 231−241.